molecules

MDPI

Article

Magnetic and Luminescence Properties of 8-Coordinate Holmium(III) Complexes Containing 4,4,4-Trifluoro-1-Phenyl- and 1-(Naphthalen-2-yl)-1,3-Butanedionates

Franz A. Mautner [1,*], Florian Bierbaumer [1], Ramon Vicente [2], Saskia Speed [2], Ánnia Tubau [2], Mercè Font-Bardía [3], Roland C. Fischer [4] and Salah S. Massoud [5,6,*]

[1] Institute of Physical and Theoretical Chemistry, Graz University of Technology, Stremayrgasse 9, A-8010 Graz, Austria; bierbaumerflorian97@gmail.com
[2] Departament de Química Inorgànica i Orgànica, Universitat de Barcelona, Martí i Franquès 1-11, E-08028 Barcelona, Spain; rvicente@ub.edu (R.V.); saskia.speed@qi.ub.es (S.S.); anniatubau@ub.edu (Á.T.)
[3] Departament de Mineralogia, Cristallografia i Dipòsits Minerals and Unitat de Difracció de R-X, Centre Científic i Tecnològic de la Universitat de Barcelona (CCiTUB), Universitat de Barcelona, Solé i Sabarís 1–3, 08028 Barcelona, Spain; mercefont@ub.edu
[4] Institute of Inorganic Chemistry, Graz University of Technology, Stremayrgasse 9, A-8010 Graz, Austria; roland.fischer@tugraz.at
[5] Department of Chemistry, University of Louisiana at Lafayette, P.O. Box 43700, Lafayette, LA 70504, USA
[6] Department of Chemistry, Faculty of Sciences, Alexandria University, Moharam Bey, Alexandria 21511, Egypt
* Correspondence: mautner@tugraz.at (F.A.M.); ssmassoud@louisiana.edu (S.S.M.); Tel.: +43-316-873-32270 (F.A.M.); +1-337-482–5672 (S.S.M.); Fax: +43-316-873-8225 (F.A.M.); +1-337-482–5676 (S.S.M.)

check for updates

Citation: Mautner, F.A.; Bierbaumer, F.; Vicente, R.; Speed, S.; Tubau, Á.; Font-Bardía, M.; Fischer, R.C.; Massoud, S.S. Magnetic and Luminescence Properties of 8-Coordinate Holmium(III) Complexes Containing 4,4,4-Trifluoro-1-Phenyl- and 1-(Naphthalen-2-yl)-1,3-Butanedionates. *Molecules* **2022**, *27*, 1129. https://doi.org/10.3390/molecules27031129

Academic Editor: Hiroshi Sakiyama

Received: 29 December 2021
Accepted: 4 February 2022
Published: 8 February 2022

Abstract: A new series of mononuclear Ho^{3+} complexes derived from the β-diketonate anions: 4,4,4-trifluoro-1-phenyl-1,3-butanedioneate ($btfa^-$) and 4,4,4-trifuoro-1-(naphthalen-2-yl)-1,3-butanedionate ($ntfa^-$) have been synthesized, $[Ho(btfa)_3(H_2O)_2]$ (**1a**), $[Ho(ntfa)_3(MeOH)_2]$ (**1b**), (**1**), $[Ho(btfa)_3(phen)]$ (**2**), $[Ho(btfa)_3(bipy)]$ (**3**), $[Ho(btfa)_3(di\text{-}^tbubipy)]$ (**4**), $[Ho(ntfa)_3(Me_2bipy)]$ (**5**), and $[Ho(ntfa)_3(bipy)]$ (**6**), where phen is 1,10-phenantroline, bipy is 2,2′-bipyridyl, di-^{t}bubipy is 4,4′-di-*tert*-butyl-2,2′-bipyridyl, and Me_2bipy is 4,4′-dimethyl-2,2′-bipyridyl. These compounds have been characterized by elemental microanalysis and infrared spectroscopy as well as single-crystal X-ray difraction for **2**–**6**. The central Ho^{3+} ions in these compounds display coordination number 8. The luminescence-emission properties of the pyridyl adducts **2**–**6** display a strong characteristic band in the visible region at 661 nm and a series of bands in the NIR region (excitation wavelengths (λ_{ex}) of 367 nm for **2**–**4** and 380 nm for **5** and **6**). The magnetic properties of the complexes revealed magnetically uncoupled Ho^{3+} compounds with no field-induced, single-molecule magnet (SMMs).

Keywords: lanthanides; holmium; X-ray; diketones; magnetic properties; luminescence

1. Introduction

The luminescent emissions of lanthanides in general, and specifically holmium complexes, have been known for decades, as they play crucial roles in research and have a wide range of useful applications [1–28]. Compared to other lanthanides, holmium was proved to serve as a good candidate to make quantum computers, where one bit of data can be stored on a single holmium atom set on a bed of magnesium oxide [23,24]. In addition, Ho is used to generate the strongest artificial magnetic fields when placed within high-strength magnets [25]; Ho-dopped yttrium iron garnet is used in optical insulators, microwave equipment, and in solid-state lasers [26], and is one of the colorant's sources for yellow and red colors in glass and cubic zirconia [27].

Lanthanide ions, Ln^{3+} and their complexes, are known to exhibit narrow and characteristic *f*–*f* transitions of luminescent emissions that span from ultraviolet (UV) to visible and near-infrared (NIR) regions [1–3,29–32]. The *f*–*f* transitions in Ln^{3+} complexes are weak,

but this process is enhanced via effective energy transfer from ligands or linker electrons to the central metal ions "antenna effect", from which the emission occurs [1–3,20,21,32–35]. Most of the investigated complexes, such as Eu^{3+} and Tb^{3+}, emit red or green luminescent light, respectively [36–39], but other Ln^{3+} complexes, such as those containing $Yb^{3+,}$ Nd^{3+}, and Pr^{3+} metal ions, exhibit luminescence in the near-IR region [40–43].

The lanthanide cations (Ln^{3+}) as hard Lewis acids exhibit a strong binding affinity for *O*-donor ligands such as β-diketone compounds (HL) [43–49]. Typically electrically neutral tris complexes, $Ln(L)_3$ are most likely to be formed [40–55], but in some cases, the anionic tetrakis complexes, $(Cat^+)[Ln(L)_4]^-$ are also formed [49,56–59]. The two categories of these compounds exhibit good luminescent properties [40–59]. The luminescence efficiency of the β-diketonato complexes can be enhanced by the appropriate choice of the substituents on the β-diketone ligand because, in this way, the ligands' triplet levels can be tuned to provide efficient energy transfer between the diketonato ligand and the lanthanide ion [60–63]. This has been observed when aromatic and fluorinated alkyl groups are incorporated into the β-diketone skeletons. This helps in reducing the nonradiative quenching of lanthanide luminescence [40–42,50–63]. In the anionic $(Cat^+)[Ln(L)_4]$ complexes, additional tuning of the photophysical properties is possible by changing the counterion, Cat^+, which in turn changes the structure of the complex and, in particular, the local coordination geometry of the metal ion [56–59].

The rare-earth complexes with fluorinated-β-diketones (HL), such as L = 4,4,4-trifluoro-1-phenyl-1,3-butanedionate (btfa) and 4,4,4-trifuoro-1-(naphthalen-2-yl)-butane-1,3-dionate (L = ntfa) anions, have been extensively investigated. The structure formulas of H(btfa) and H(ntfa) are shown in Scheme 1. Among the Ln(III)-btfa complexes, half of them are for Eu(III) compounds [52–57,59,62–64], whereas the rest are for Dy(III) [50,51,60], Er(III) [55,61], Tb(III) [62], and Gd(III) [56,63]. In addition, small numbers were reported for Sm(III) [58], Pr(III) [42], and Ho(III) [65]. No structural results were found for La(III), Ce(III), Nd(III), Yb(III), nor Lu(III). In case of Ln(III)-ntfa, less structures were reported compared to the corresponding Ln(III)-btfa compounds, where most were obtained with Eu(III) [38–41,55,56,60–66], Gd(III) [43,53,55–57,66], and Pr(III) [42,45,48,65], some with Dy(III) [50,60,66] and Er(III) [55,65], as well as Tb(III) [62,66]. To the best of our knowledge, few structures were characterized with La(III) [49], Nd(III) [43], Ho(III) [65], and Sm(III) [65], but no structures for Ce(III), Yb(III), nor Lu(III) were found.

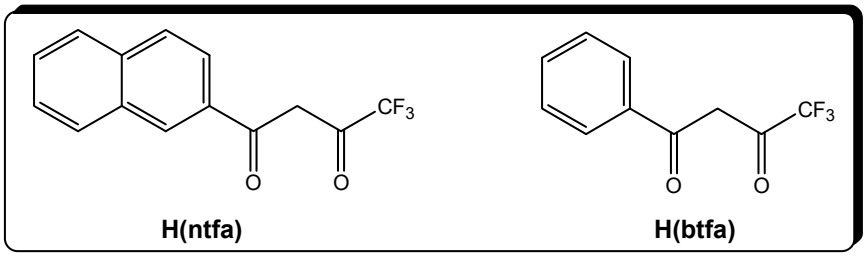

Scheme 1. Structures of the β-diketones used in this study.

As part of a long project to explore the coordination properties and the physicochemical properties of the less-studied Ln^{3+} ions with the β-diketones, Ho(btf) and Ho(ntfa), the following studies were undertaken and devoted for the interaction of these two compounds with Ho^{3+} ions in the presence of different polypyridyl ligands.

2. Materials and Methods

2.1. Materials and Physical Measurements

4,4,4-Trifluoro-1-(phenyl)butane-1,3-dione, 4,4,4-trifluoro-1-(naphthalen-2-yl)-butane-1,3-dione, 4,4′-di-*tert*-butyl-2,2′-bipyridine, 5,5′-dimethyl-2,2′-bipyridine, and 2,2′-bipyridine were purchased from TCI, and the other chemicals were of analytical grade quality. Infrared spectra of solid complexes were either recorded on a Bruker Alpha P (platinum-ATR-cap) spectrometer (Bruker AXS, Madison, WI, USA) or a Thermo Scientific Nicolet IS5 spec-

trophotometer. Elemental microanalyses were carried out with an Elementar Vario EN3 analyzer (Langenselbold, Germany) at the Serveis Científics i Tecnològics of the Universitat de Barcelona. PXRD patterns were recorded with a Bruker D8 Advance powder diffractometer (Cu-Kα radiation) (Bruker AXS, Madison, WI, USA).

Solid-state fluorescence spectra of compounds **2**–**6** were recorded on a Horiba Jobin Yvon SPEX Nanolog fluorescence spectrophotometer (Fluorolog-3 v3.2, HORIBA Jovin Yvon, Cedex, France) equipped with a three-slit, double-grating excitation and emission monochromator with dispersions of 2.1 nm/mm (1200 grooves/mm) at room temperature. The steady-state luminescence was excited by unpolarized light from a 450 W xenon CW lamp and detected at an angle of 22.5° for solid-state measurement by a red-sensitive Hamamatsu R928 photomultiplier tube. Near Infra-red (NIR) spectra were recorded at an angle of 22.5° using a liquid-nitrogen-cooled, solid indium/gallium/arsenic detector (900–1600 nm). The instrument was adjusted to obtain the highest background-to-noise ratio with a band pass of 2 for the visible and 10 for the NIR measurements. The sample was mounted between two quartz plates. Spectra were corrected for both the excitation source light intensity variation (lamp and grating) and the emission spectral response (detector and grating).

The magnetic susceptibility and magnetization measurements were performed with a Quantum Design MPMS-XL SQUID magnetometer at the Magnetic Measurements Unit of the University of Barcelona. Pascal's constants were used to estimate the diamagnetic corrections, which were subtracted from the experimental susceptibilities to give the corrected molar magnetic susceptibilities.

2.2. Synthesis of the Complexes

2.2.1. $[Ho(btfa)_3(H_2O)_2]$ (**1a**)

To a methanol solution (10 mL) containing NaOH (6 mmol, 0.240 g), Hbtfa was added in an amount of 6 mmol, 0.130 g, and $HoCl_3{\cdot}6H_2O$ was added in an amount of 2 mmol, 0.759 g. The solution was stirred for 1 h at room temperature, then 80 mL of deionized water was added to the reaction mixture and stirred overnight. The light pink precipitate, which was obtained, was filtrated and dried in a desiccator overnight (yield: 1.194 g, 71%), Anal. Calcd. for $C_{30}H_{22}F_9HoO_8$ (846.4 g/mol): C, 42.6; H, 2.6%. Found: C, 42.5; H, 2.7%. Selected IR bands (cm^{-1}): 3658 (m), 3462 (br), 1609 (s), 1575 (s), 1527 (m), 1488 (m), 1464 (m), 1329 (s), 1283 (s), 1245 (m), 1182 (s), 1144 (s), 1071(m), 945 (m), 777 (m), 694 (m), 631(m), 580 (m).

2.2.2. $[Ho(ntfa)_3(MeOH)_2]$ (**1b**)

A methanolic solution (10 mL) of $Ho(NO_3)_3\ 5H_2O$ (281 mg, 0.64 mmol) and a methanolic solution (20 mL) of 4,4,4-trifluoro-1-(2-naphthyl)-1,3-butanedione (515 mg, 1.93 mmol) with 1M NaOH (2.0 mL) were dissolved. After 20 min of stirring, the 4,4,4-trifluoro-1-(2-naphthyl)-1,3-butanedione solution was added to the $Ho(NO_3)_3\ 5H_2O$ solution. After 3 h of stirring, 30 mL of deionized water was added to complete the reaction. The mixture was stirred for 12 h at ambient temperature and then filtered. The obtained white powder was re-crystallized from MeOH and dried at 60 °C for 30 min (yield: 509 mg, 81%). Characterization: Anal. Calcd. for: $C_{44}H_{32}F_9HoO_8$ (1018.62 g/mol): C, 51.9; H, 3.2%. Found: C, 51.8; H, 3.1%. Selected IR bands (ATR-IR, cm^{-1}): 3448 (m, br), 1602 (s), 1594 (m), 1568 (m), 1529 (m), 1458 (w), 1356 (w), 1285 (s), 1251 (m), 1184 (s), 1124 (s), 1073 (w), 958 (w), 865 (w), 824 (w), 794 (s), 762 (w), 684 (w).

2.2.3. $[Ho(btfa)_3(L)]$ (**2**: L = phen; **3**: L = bipy; **4**: L = di-^{t}Bubipy)

A general method was used to prepare the complexes **2**–**4**. An ethanol solution (15 mL) containing bipyridyl derivatives (1 mmol, **2**: 0.180 g 1,10-phenanthroline; **3**: 0.156 g 2,2′-bipyridine; **4**: 0.846 g 4,4′-di-*tert*-butyl-2,2′-bipyridine) was added to another ethanol solution (15 mL) containing $[Ho(btfa)_3(H_2O)_2]$ (1 mmol, 0.846 g). The solution was stirred for 30 min and then left to stand at room temperature. Single light pink crystals suitable for

X-ray diffraction were obtained within a week. These were collected by filtration and dried with air.

[Ho(btfa)$_3$(phen)] (**2**) (yield: 38%). Characterization: Anal. Calcd. for $C_{42}H_{26}F_9HoN_2O_6$ (990.58 g/mol): C, 50.9; H, 2.6; N, 2.8%. Found: C, 50.7; H, 2.5; N, 2.8%. Selected IR bands (cm^{-1}): 1610 (s), 1574 (s), 1522 (s), 1483 (m), 1476 (m), 1319 (m), 1291 (s), 1246 (m), 1178 (s), 1134 (s) 1077 (m), 846 (m), 763 (s), 770 (s), 631 (m), 580 (m).

[Ho(btfa)$_3$(bipy)] (**3**) (yield: 80%). Characterization: Anal. Calcd. for $C_{40}H_{26}F_9HoN_2O_6$ (966.56 g/mol): C, 49.7; H, 2.7; N, 2.9%. Found: C, 49.7; H, 2.5; N, 2.8%. Selected IR bands (cm^{-1}): 1606 (s), 1569 (s), 1533 (m), 1472 (m), 1320 (m), 1279 (s), 1242 (m), 1177 (s), 1122 (s), 1067 (m), 1016 (m), 947 (m), 758 (s), 688 (s), 624 (s).

[Ho(btfa)$_3$(di-^{t}bubipy)] (**4**) (yield: 23%). Characterization: Anal. Calcd. for $C_{48}H_{42}F_9HoN_2O_6$ (1078.77 g/mol): C, 53.4; H, 3.9; N, 2.6%. Found: C, 53.3; H, 3.7; N, 2.7%. Selected IR bands (cm^{-1}): 2971 (w), 1612 (s), 1576 (m), 1539 (m), 1479 (m), 1403 (w), 1321 (m), 129 (s), 1248 (m), 1181 (s), 1127 (s), 1075 (m), 1026 (w), 948 (w), 848 (w), 766 (s), 699 (s), 635 (s), 580 (s).

2.2.4. [Ho(ntfa)$_3$(5,5′-Me$_2$bipy)] (**5**)

[Ho(ntfa)$_3$(MeOH)$_2$] (127 mg, 0.125 mmol) and 5,5′-Dimethyl-2,2′-dipyridyl (28 mg, 0.15 mmol) were dissolved in 30 mL ethanol/acetone (3:1). The solution was stirred for approximately for 2 h. The mixture was filtered, and the mother liquor was left in an open atmosphere. After two weeks, pink crystals of **5** were obtained from the mother liquor (yield: 43 mg, 30%). Characterization: Anal. Calcd. for: $C_{54}H_{36}F_9HoN_2O_6$ (1144.78 g/mol): C, 56.7; H, 3.2; N, 2.4%. Found: C, 56.6; H, 3.1; N, 2.5%. Selected IR bands (ATR-IR, cm^{-1}): 1738 (w), 1608 (s), 1590 (m), 1566 (m), 1526 (m), 1506 (m), 1476 (w), 1384 (w), 1353 (w), 1284 (s), 1217 (w), 1183 (m), 1131 (s), 1073 (w), 956 (m), 935 (w), 862 (w), 790 (s), 748 (m), 681 (m), 569 (m), 517 (w), 467 (m), 416 (w).

2.2.5. [Ho(ntfa)$_3$(bipy)] (**6**)

[Ho(ntfa)$_3$(MeOH)$_2$] (124 mg, 0.122 mmol) was dissolved in 15 mL ethanol/acetone (4:1). 2,2´-bipyridyl (28 mg, 0.18 mmol) was dissolved in 15 mL ethanol/acetone (4:1). The solutions were combined and stirred approximately for 2 h. The mixture was filtered, and the mother liquor was left in an open atmosphere. After ten days, light pink crystals of **6** were obtained from the mother liquor (yield: 37 mg, 29%). Characterization of solvent-free compound: Anal. Calcd. for: $C_{52}H_{32}F_9HoN_2O_6$ (1116.73 g/mol): C, 55.9; H, 2.9; N, 2.5%. Found: C, 55.8; H, 2.8; N, 2.6%. Selected IR bands (ATR-IR, cm^{-1}): 1610 (s), 1591 (m), 1568 (m), 1528 (m), 1507 (m), 1460 (m), 1437 (w), 1387 (w), 1354 (w), 1286 (s), 1188 (m), 1121 (s), 1075 (w), 958 (m), 865 (w), 790 (s), 760 (m), 682 (w), 568 (m), 518 (w), 470 (m), 414 (w).

2.3. X-Ray Crystal Structure Analysis

Single crystals of **2**–**4** were set up in air on a Bruker-AXS D8 VENTURE diffractometer with a CMOS detector of **5** and **6** on a Bruker-AXS APEX II diffractometer (Bruker-AXS; Madison, WI, USA). The crystallographic data and details of the refinement are listed in Table 1. All the structures were refined by the least-squares method. Intensities were collected with multilayer monochromated Mo-Kα radiation. Lorentz polarization and absorption corrections were made in all the samples [67,68]. The structures were solved by direct methods using the SHELXS-97 computer program and refined by full-matrix least-squares method using the SHELXL-2014 computer program [69,70]. The non-hydrogen atoms were located in successive difference Fourier syntheses and refined with anisotropic thermal parameters on F^2. Isotropic temperature factors were assigned as 1.2 or 1.5 times the respective parent for hydrogen atoms. For **6**, a SQUEEZE treatment was used to eliminate disordered solvent molecules. Further programs used: Mercury [71] and PLATON [72]. CCDC 2120112-2120116 contains the supplementary crystallographic data for **2**–**6**, respectively.

Table 1. Crystal data and details of the structure determination of compounds **2**–**6**.

Compound	2	3	4	5	6
Empirical formula	$C_{42}H_{26}F_9HoN_2O_6$	$C_{40}H_{26}F_9HoN_2O_6$	$C_{48}H_{42}F_9HoN_2O_6$	$C_{54}H_{36}F_9HoN_2O_6$	$C_{52}H_{32}F_9HoN_2O_6$
Formula mass	990.58	966.56	1078.76	1144.78	1116.73
System	Monoclinic	Monoclinic	Triclinic	Orthorhombic	Orthorhombic
Space group	P21/c	P21/n	P-1	Pca21	Pna21
a (Å)	9.6058(7)	11.0408(10)	12.3569(16)	20.2138(9)	20.7013(6)
b (Å)	36.627(2)	22.6440(18)	13.6076(18)	11.7503(5)	10.9059(3)
c (Å)	10.7464(7)	15.2463(13)	14.3853(18)	19.5852(7)	42.3027(10)
α (°)	90	90	92.478(5)	90	90
β (°)	92.932(3)	101.972(3)	99.883(5)	90	90
γ (°)	90	90	105.233(5)	90	90
V (Å3)	3776.0(4)	3728.8(6)	2289.3(5)	4651.8(3)	9550.5(4)
Z	4	4	2	4	8
μ (mm^{-1})	2.192	2.218	1.815	1.792	1.744
D_{calc} (Mg/m^3)	1.742	1.722	1.565	1.635	1.553
θ max (°)	26.420	34.495	27.171	28.998	28.000
Data collected	91277	103169	50752	93718	264468
Unique refl./R_{int}	7737/0.0836	15617/0.0776	10082/0.0390	12315/0.0812	23060/0.0515
Parameters/Restraints	542/0	523/0	601/0	651/1	1262/19
Goodness-of-fit on F^2	1.120	1.050	1.131	1.012	1.165
R1/wR2 (all data)	0.0615/0.1342	0.0466/0.0809	0.0445/0.1042	0.0374/0.0632	0.0466/0.1060

3. Results and Discussion

3.1. Synthesis and IR Spectra of the Complexes

The precursor complexes $[Ho(btfa)_3(H_2O)_2]$ (**1a**) and $[Ho(ntfa)_3(MeOH)_2]$ (**1b**) were prepared by the reaction of methanolic solutions containing Ho(III) salts, beta-dicetonate molecules (Hbtfa) or (Hntfa), respectively, and NaOH in the stoichiometric ratio 1:3:3, followed by stirring the resulting solution in H_2O. The PXRD pattern confirmed that **1a** is isostructural with $[La(btfa)_3(H_2O)_2]$ [47] and **1b** is isostructural with $[Pr(nfa)_3(MeOH)_2]$ [48]. The interaction of $[Ho(btfa)_3(H_2O)_2]$ with poly-pyridyl compounds phen, bipy, and di-^{t}bubipy in EtOH afforded the light-pink crystalline adducts $[Ho(btfa)_3(phen)]$ (**2**), $[Ho(btfa)_3$-$(bipy)]$ (**3**), and $[Ho(btfa)_3(di\text{-}^tbubipy)]$ (**4**), respectively, whereas the interaction of $[Ho(ntfa)_3$-$(MeOH)_2]$ with poly-pyridyl compounds 5,5′-Me_2bipy and bipy in ethanol/acetone mixtures afforded the crystalline adducts $[Ho(ntfa)_3(5,5'\text{-}Me_2bipy)]$ (**5**) and $[Ho(ntfa)_3(bipy)]$ (**6**) with reasonable yields (38–80%). The approach used here for the synthesis of complexes **2**–**6** is similar to that successfully employed in similar Ln(III) (Ln = La, Pr, Nd) mono bipyridyl adducts [47–49]. The isolated complexes were structurally characterized by elemental microanalyses and by IR spectroscopy, as well as by single-crystal X-ray crystallography for **2**–**6**.

The IR spectra of complexes **2**–**6** display general characteristic features. The strong vibrational band observed over the frequency range 1605–1615 cm^{-1} is typically assigned to the coordinated carbonyl stretching frequency, ν(C=O) [47–49]. The broad band centered at 3462 cm^{-1} in **1a** and 3448 cm^{-1} in **1b** is assigned to the ν(O-H) stretching frequency of the coordinated aqua/methanol ligands.

*3.2. Description of the Crystal Structures **2**–**6***

Molecular plots and coordination figures of **2**–**6** complexes are depicted in Figures 1–5, and selected bond parameters are summarized in Table 2. Each Ho(III) center of the neutral and monomeric complex **2**–**6** are ligated by six oxygen donor atoms of three β-diketonato ligands anions ($btfa^-$) for **2**–**4** or ($ntfa^-$) for **5** and **6**, respectively, in the chelating coordination mode. The coordination number (CN) 8 in **2** is completed by two *N*-donor atoms of one phen chelating ligand. The Ho-N/O bond lengths in **2** are in the range of 2.3051(2)–2.5549(2) Å. The CN = 8 in **3**–**6** of the HoO_6N_2 coordination sphere around Ho

is achieved by the ligation of one 2,2′-bipy (**3** and **6**), di-^{t}Bu-bipy (**4**), and 5,5′-Me2-bipy (**5**) chelating ligands, respectively. The Ho-N/O bond lengths for **3** are in the range of 2.287(2)-2.527(3) Å, for **4**, from 2.292(3) to 2.541(4) Å, for **5**, from 2.293(4) to 2.518(4) Å, and for **6**, from 2.268(6) to 2.530(7) Å, respectively. The O-Ho-O bite angles of the β-diketonato groups fall in the range from 71.5(2) to 76.21(1)° in **2**–**6**, whereas the corresponding N-Ho-N bite angles of the chelating phen, bipy, di-^{t}bu-bipy, and 5,5′-Me_2bipy ligands in compounds **2**–**6** vary from 63.80(13) to 64.66(1)°.

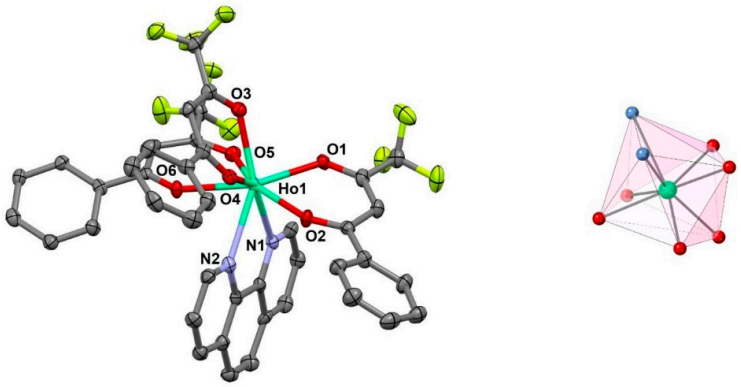

Figure 1. Left: partially labeled structure [Ho(btfa)$_3$(phen)] (**2**). Color code: turquoise = Ho, red = O, yellow = F, grey = C. Right: coordination polyhedron of Ho(III) ion in compound **2**.

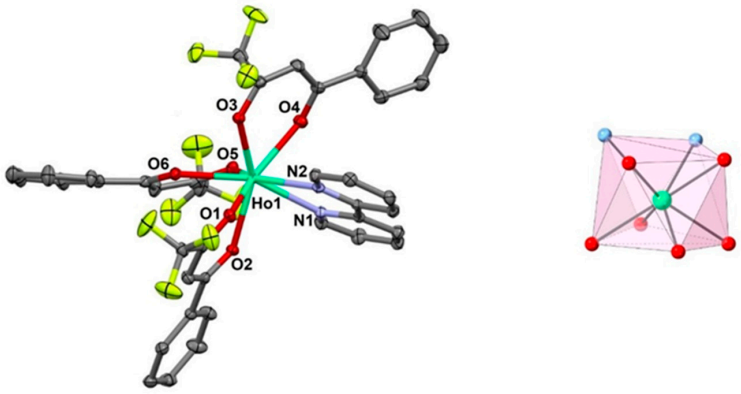

Figure 2. Left: partially labeled structure [Ho(btfa)$_3$(bipy)] (**3**). Color code: turquoise = Ho, red = O, yellow = F, blue = N, grey = C. Right: coordination polyhedron of Ho(III) ion in compound **3**.

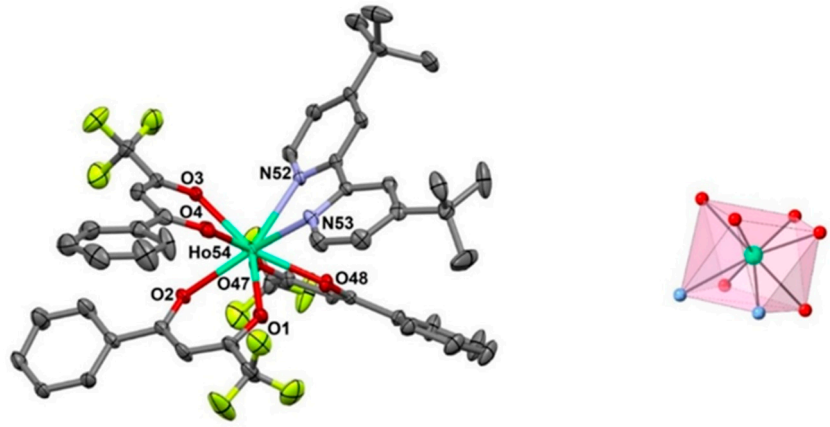

Figure 3. Left: partially labeled structure [Ho(btfa)$_3$(di-^{t}bubipy)] (**4**). Color code: turquoise = Ho, red = O, yellow = F, blue = N, grey = C. Right: coordination polyhedron of Ho(III) ion in compound **4**.

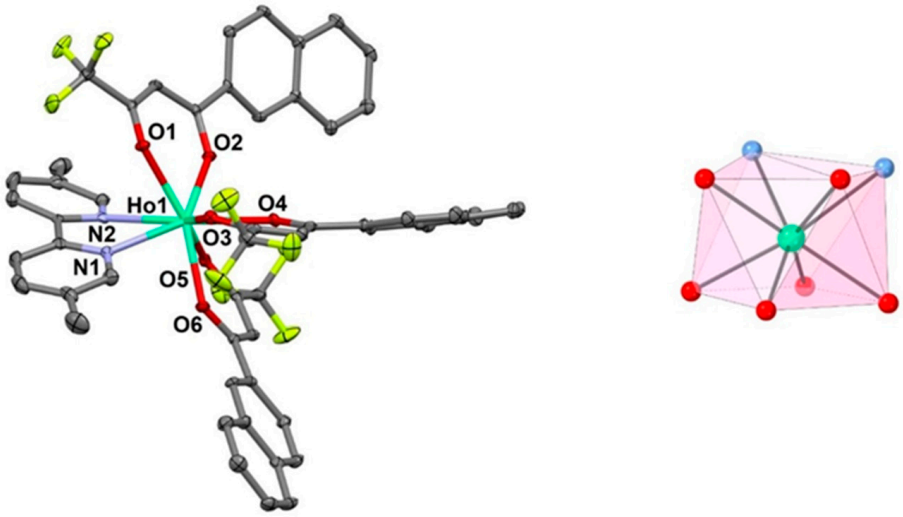

Figure 4. Left: partially labeled structure [Ho(ntfa)$_3$(5,5′-Me$_2$-bipy)] (**5**). Color code: turquoise = Ho, red = O, yellow = F, blue = N, grey = C. Right: coordination polyhedron of Ho(III) ion in compound **5**.

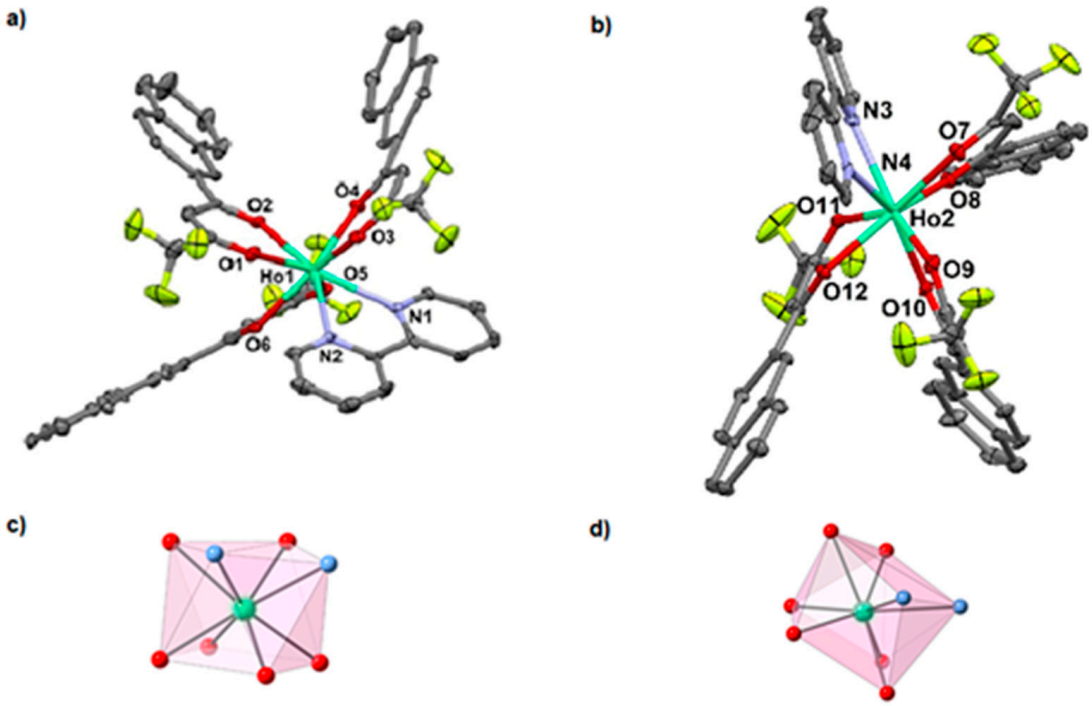

Figure 5. (**a**) Partially labeled structure **of** [Ho(ntfa)$_3$(bipy)] (**6**): (**a**) Ho atom 1, (**b**) Ho atom 2, (**c**) coordination polyhedron of Ho atom1 and (**d**) coordination polyhedron of Ho atom 2. Color code: turquoise = Ho, red = O, yellow = F, blue = N, grey = C.

Table 2. Selected bond distances (Å) and bite angles (°) for compounds **2**–**6**.

Compound 2		**Compound 3**		**Compound 4**	
Ho1-O1	2.3111(2)	Ho1-O1	2.315(2)	Ho54-O1	2.292(3)
Ho1-O2	2.3051(2)	Ho1-O2	2.343(2)	Ho54-O2	2.331(3)
Ho1-O3	2.3064(2)	Ho1-O3	2.297(2)	Ho54-O3	2.323(3)
Ho1-O4	2.3139(2)	Ho1-O4	2.326(2)	Ho54-O4	2.320(3)
Ho1-O5	2.3647(2)	Ho1-O5	2.287(2)	Ho54-O47	2.305(3)
Ho1-O6	2.3225(2)	Ho1-O6	2.330(2)	Ho54-O48	2.323(3)
Ho1-N1	2.5477(2)	Ho1-N1	2.524(2)	Ho54-N52	2.535(4)
Ho1-N2	2.5549(2)	Ho1-N2	2.527(3)	Ho54-N53	2.541(4)
O1-Ho1-O2	72.59(1)	O1-Ho1-O2	72.58(7)	O1-Ho54-O2	73.50(11)
O3-Ho1-O5	72.74(1)	O3-Ho1-O4	72.69(3)	O3-Ho54-O4	73.70(13)
O4-Ho1-O6	76.21(1)	O5-Ho1-O6	73.61(8)	O47-Ho54-O48	72.77(11)
N1-Ho1-N2	64.66(1)	N1-Ho1-N2	63.89(8)	N52-Ho54-N53	63.80(13)
Compound 5				**Compound 6**	
Ho1-O1	2.336(4)	Ho1-O1	2.273(6)	Ho2-O7	2.342(6)
Ho1-O2	2.293(4)	Ho1-O2	2.323(6)	Ho2-O8	2.285(6)
Ho1-O3	2.321(4)	Ho1-O3	2.362(6)	Ho2-O9	2.283(6)
Ho1-O4	2.311(4)	Ho1-O4	2.268(6)	Ho2-O10	2.319(6)
Ho1-O5	2.328(4)	Ho1-O5	2.320(6)	Ho2-O11	2.337(6)
Ho1-O6	2.313(4)	Ho1-O6	2.318(6)	Ho2-O12	2.341(6)
Ho1-N1	2.515(5)	Ho1-N1	2.495(7)	Ho2-N3	2.511(7)
Ho1-N2	2.518(4)	Ho1-N2	2.530(7)	Ho2-N4	2.516(7)
O1-Ho1-O2	71.77(13)	O1-Ho1-O2	73.8(2)	O7-Ho2-O8	72.1(2)
O3-Ho1-O4	72.95(12)	O3-Ho1-O4	71.5(2)	O9-Ho2-O10	73.5(2)
O5-Ho1-O6	72.37(13)	O5-Ho1-O6	72.7(2)	O11-Ho2-O12	72.0(2)
N1-Ho1-N2	64.38(16)	N1-Ho1-N2	64.5(3)	N3-Ho2-N4	64.6(2)

Various non-covalent interactions (ring···ring, C-H(X)···ring [72], hydrogen bonds) are summarized in Tables S1–S5 for compounds **2**–**6**, respectively.

In order to analyze the degree of distortion of the coordination polyhedra for compounds **2**–**6** from their ideal polyhedron geometry, calculations using the continuous shape measures theory with the SHAPE software were performed [73,74]. The HoO_6N_2 coordination polyhedron of **2**–**6** shows an intermediate distortion between various ideal eight-vertex polyhedra geometries. These are a square antiprism (SPAR-8), triangular dodecahedron (TDD-8), and biaugmented trigonal prism (BTPR-8) with continuous shape values of 1.382, 1.236, and 1.779 for **2**; 0.553, 2.351, and 2.051 for **3**; 0.417, 2.515, and 2.254 for **4;** and 0.497, 2.210, and 1.958 for **5**.

The corresponding calculations of the degree of distortion of the HoO_6N_2 coordination polyhedra of compound **6** [(Ho(ntfa)$_3$(bipy)] reveals an intermediate distortion between various coordination polyhedra geometries. These are a square antiprism (SPAR-8), triangular dodecahedron (TDD-8), and biaugmented trigonal prism (BTPR-8) with continuous shape measures values of 0.412, 2.348, and 2.33 for $Ho(1)O_6N_2$ and 0.3944, 2.165, and 2.115 for $Ho(2)O_6N_2$.

3.3. Photoluminescence of the Complexes

The luminescence spectra of compounds **2**–**6** were measured in the solid state at room temperature. The excitation spectra recorded at the emission wavelength (λ_{em}) of 661 nm reveal a broad, intense band around 367 nm for **2**–**4** and 380 nm for **5** and **6**. This broad band corresponds to the $\pi \rightarrow \pi^*$ transition from the ligands. The luminescence emission spectra of the samples were recorded upon the excitation wavelengths (λ_{ex}) of 367 nm for **2**–**4** and 380 nm for **5** and **6**. All spectra display a characteristic band at 661 nm ($^5F_5 \rightarrow {}^5I_8$) corresponding to the metal-centered emission and is assigned to the Ho^{3+} *f-f* transition from the $^5F_5$ excited state to the $^5I_8$ ground state. For this band, the Stark splitting of the degenerate 4*f* levels under the crystal field is perceived. In addition, compounds **2**–**4**

showed a weak band at 545 nm, which can be assigned to an *f-f* transition from higher-energy states ($^5F_4$, $^5S_2$) to the ground state $^5I_8$ [75–77]. The triplet states of the ntfa and btfa ligands were calculated by Sato and Wadain Gd(III) complexes [78], taking into account the sensitization effect of the energy transfer from the singlet state of the ligand (S_1) to the lower-in-energy ligand triplet state (T_1) through the intersystem crossing. These calculations showed that the ntfa T_1 state falls around 19,600 cm^{-1} for ntfa and 21,400 cm^{-1} for btfa. Thus, we can suggest that the energy transfer from the T_1 of the ntfa ligand to the $^5F_4$ and $^5S_2$ (18,348 cm^{-1}) thermal state is inefficient because the two states are too close in energy, and as a result, the $^5F_4$, $^5S_2 \rightarrow {}^5I_8$ transitions are not identified for compounds **5** and **6**, but they are seen for btfa complexes **2**–**4** [79]. Typical representative UV-Vis and luminescence emission spectra (Vis and NIR regions) are depicted in Figure 6 for **3** and Figure 7 for **6** as representatives of the two categories of **2**–**4** and **5** and **6** complexes, respectively (for luminescence spectra of **2**, **4**, and **5**, see Figures S12–S14).

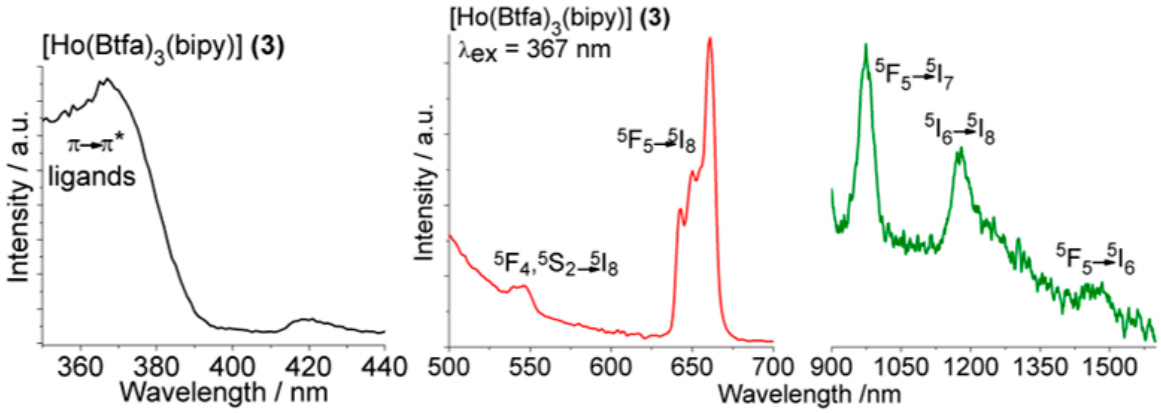

Figure 6. Spectra for complex **3**. Luminescence excitation (**black line**), emission in the visible range (**red line**), and in the NIR (**green line**) regions.

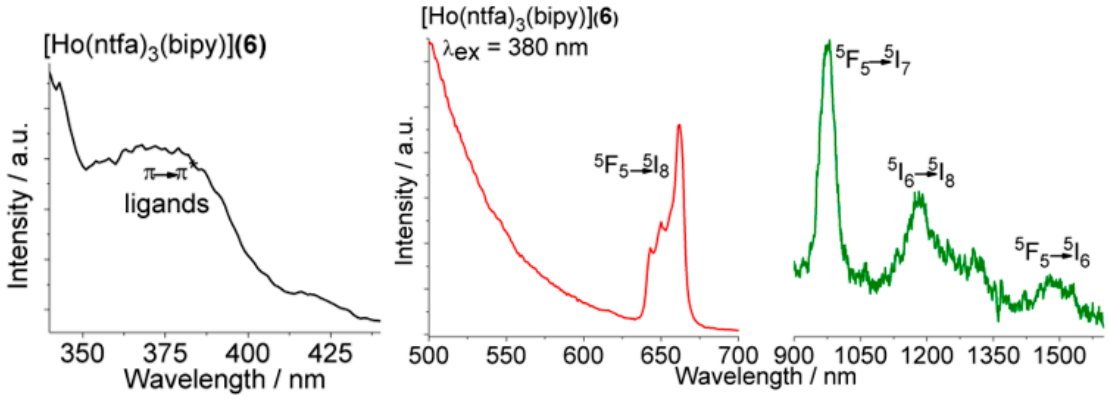

Figure 7. Spectra for complex **6**. Luminescence excitation (**black line**), emission in the visible (**red line**), and in the NIR (**green line**) regions.

Furthermore, the luminescence emissions of the compounds **2**–**6** were recorded in the NIR region from 900 to 1600 nm, where three weak bands were detected at 973, 1179, and 1474 nm. The first and most intense band is assigned to the $^5F_5 \rightarrow {}^5I_7$ transition. The band located at 1179 nm accounts for the $^5I_6 \rightarrow {}^5I_8$ transition; the very weak band at 1474 nm corresponds to the $^5F_5 \rightarrow {}^5I_6$ transition [80]. The results obtained here agree with other Ho(III) coordination compounds, where the study of the sensitization of Ho^{3+} luminescence by the energy transfer from chromophore ligands has been performed [81–85].

3.4. Magnetic Properties of the Complexes

3.4.1. Ac Magnetic Susceptibility Studies

In order to study the dynamic magnetic properties and the possible Single Molecular Magnet (SMM) behavior (slow relaxation of magnetization) of the synthesized compounds, ac magnetic susceptibility, measurements were recorded for solvent-free compounds **2**–**5**. Compounds **2**–**5** do not show a dependence on the in-phase and out-of-phase components in front of the temperature and frequency, neither in the minimum dc field (0 T) nor in the maximum applied dc magnetic field (0.1 T). Therefore, these compounds do not show slow relaxation of the magnetization and consequently will not show SMM's behavior.

3.4.2. Dc Magnetic Susceptibility Studies

Powder samples of complexes **2**–**5** were measured under applied magnetic fields of 0.3 T (300–2 K). The data are plotted as $\chi_M T$ products versus T in Figure 8. Magnetization dependence of the applied field at 2 K for compounds **2**–**5** was also recorded and is shown in Figure 9.

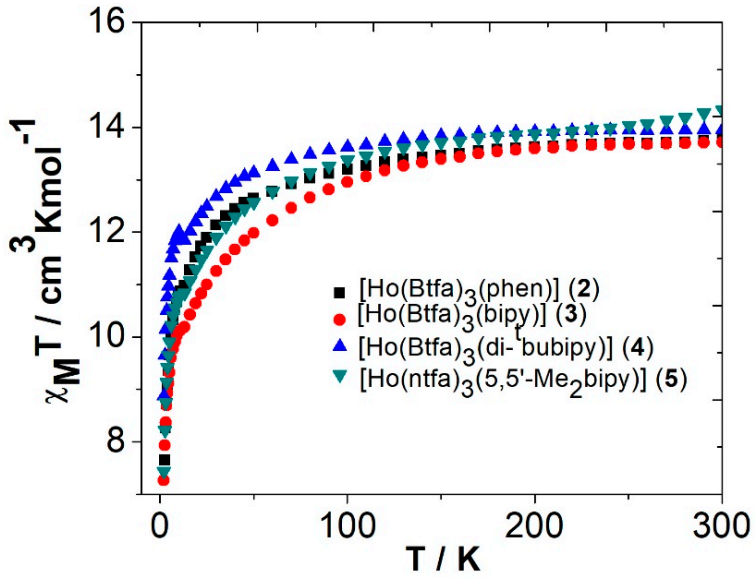

Figure 8. χ_MT vs. T plots for compounds **2**–**5**.

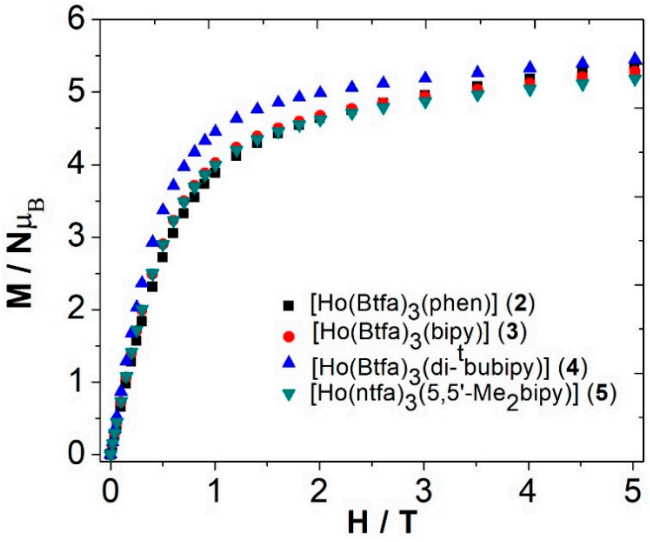

Figure 9. Field dependence of the magnetization plots at T = 2 K for compounds **2**–**5**.

The magnetic measurement on **2–5** reveals that the $\chi_M T$ values at 300 K are 13.8, 13.7, 13.9, and 14.3 cm^3 K mol^{-1}, respectively, which are in the range of the theoretical value for a magnetically uncoupled Ho(III) compound (14.07 $cm^3 \cdot K \cdot mol^{-1}$) in the $^5I_8$ ground state ($g_J = 5/4$) [86]. On cooling the samples, $\chi_M T$ values remain constant up to 125 K. Below this temperature, $\chi_M T$ values decrease to finite values of 6.8, 7.3, 8.9, and 7.4 $cm^3 \cdot K \cdot mol^{-1}$ at 2 K for compounds **2–5**, respectively. The decrease in $\chi_M T$ values at low temperatures could be due to the depopulation of the sublevels generated for the spin–orbit coupling and the ligand-field effect (Stark sublevels).

Magnetization dependence on magnetic static applied field at $T = 2$ K for complexes **2–5** (Figure 9) reveals no saturation at high fields with similar values of 5.4, 5.3, 5.4, and 5.2 $N\mu_B$ at 5 T for **2–5**, respectively. The magnetization saturation point expected for a mononuclear Ho^{3+} complex should be $\approx 4\ N_A \mu_B$.

The $1/\chi_M$ versus T plots for **2–5** are shown in Figure 10. Between 2 K and 300 K, the $1/\chi_M$ versus T plots are linear for the four compounds and well described by the Curie–Weiss law $1/\chi_M = (T-\theta)/C$, where C = 13.9 $cm^3 \cdot K \cdot mol^{-1}$ and $\theta = -4.9$ K for **2**, C = 13.9 $cm^3 \cdot K \cdot mol^{-1}$ and $\theta = -3.50$ K for **3**, C = 14.0 $cm^3 \cdot K \cdot mol^{-1}$ and $\theta = -2.3$ K for **4**, and C = 14.3 $cm^3 \cdot K \cdot mol^{-1}$ and $\theta = -4.6$ K for **5**.

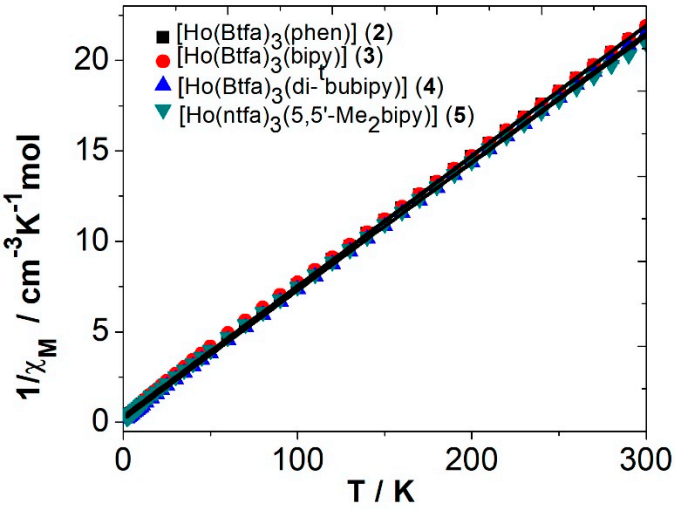

Figure 10. $1/\chi_M$ vs. T plots for compounds **2–5**. Solid lines represent the fitting using the Curie–Weiss law $1/\chi_M = (T - \theta)/C$.

4. Conclusions

A novel series of five mono-bipyridyl adducts of Ho^{3+}-trifluoro-phenyl ($btfa^-$) and -naphthalen-2-yl ($ntfa^-$) β-diketonato complexes [Ho(btfa)$_3$(phen)] (**2**), [Ho(btfa)$_3$(bipy)] (**3**), [Ho(btfa)$_3$(di-^{t}bubipy)] (**4**), [Ho(ntfa)$_3$(Me_2bipy)] (**5**), and [Ho(ntfa)$_3$(bipy)$_2$] (**6**) were synthesized from their precursors diaqua tris(β-diketonato) species. The compounds were structurally characterized, where coordination numbers CN = 8 were observed. The distortion of the coordination polyhedra of Ho^{3+} centers was analyzed with the SHAPE program. All the complexes display CN 8. In a fashion that is similar to their Ln^{3+} analog complexes (Ln = La, Pr, and Nd) derived from the same set of ligands [47–49]. The solid-state luminescence emission of the complexes revealed a strong, intense emission band at 661 nm in the visible and three other bands in NIR regions. The magnetic measurements of the complexes **2–5** revealed that the $\chi_M T$ values are within the range of 14.0 ± 0.3 $cm^3 \cdot mol^{-1} \cdot K$ at 300 K, which is predicted for a magnetically uncoupled Ho^{3+} compound (14.07 $cm^3 \cdot mol^{-1} \cdot K$) in the $^5I_8$ ground state ($g_J = 5/4$) [86]. The luminescence emission and magnetic results reported here for the Ho^{3+} compounds demonstrate that these properties are not significantly affected by either the small changes in the geometrical shape of the Ho^{3+} complexes or their local symmetry. Additionally, results are almost independent of the nature of the ancillary bipyridyl ligands or the nature of the β-diketone coligands. Similar results were

obtained with pyridyl adducts derived from the same coligands with Pr(III) and Nd(III) compounds [48,49].

Supplementary Materials: Non-covalent interactions (ring···ring, C-H(F)···ring, hydrogen bonds) are summarized in Tables S1–S5 for compounds **2**–**6**, respectively. PXRD pattern (Figure S1a,b, S2–S6), packing views (Figures S7–S11) for compounds **2**–**6**, excitation and emission spectra of compounds **2**, **4**, and **5**, recorded in the solid state at room temperature, are given in Figures S12–S14, respectively. CCDC deposition numbers: CCDC 2120112-2120116 contain the supplementary crystallographic data for **2**–**6**, respectively. These data can be obtained free of charge from The Cambridge Crystallographic Data Centre via www.ccdc.cam.ac.uk/data_request/cif.

Author Contributions: Conceptualization, F.A.M., R.V., and M.F.-B.; methodology, F.A.M., R.V. and M.F.-B.; software, F.A.M., R.C.F., M.F.-B. and R.V.; validation, F.A.M., R.V., R.C.F. and S.S.M.; formal analysis, F.B., S.S. and Á.T.; investigation, F.B., Á.T., R.C.F., M.F.-B., S.S. and R.C.F.; resources, F.A.M., R.V. and R.C.F.; data curation, F.A.M., F.B., R.C.F., R.V., M.F.-B., Á.T., S.S. and S.S.M.; writing original draft preparation, F.A.M., F.B., R.C.F., R.V., Á.T., M.F.-B., S.S. and S.S.M.; writing—review and editing, F.A.M., Á.T., R.V. and S.S.M.; visualization, F.A.M., Á.T., R.V., M.F.-B. and S.S.; supervision, F.A.M., R.V. and S.S.M.; project administration, F.A.M. and R.V.; funding acquisition, R.V. All authors have read and agreed to the published version of the manuscript.

Funding: R.V. acknowledges the financial support from MINECO Project PGC2018-094031-B-I00.

Institutional Review Board Statement: Not applicable.

Informed Consent Statement: Not applicable.

Data Availability Statement: Data is contained within the article or supplementary material.

Conflicts of Interest: The authors declare no conflict of interest.

Sample Availability: Samples of the compounds are not available.

References

1. Bünzli, J.-C.G.; McGill, I.I. Rare Earth Elements. In *Ullmann's Encyclopedia of Industrial Chemistry*; Wiley: Hoboken, NJ, USA, 2018; pp. 1–53.
2. Bünzli, J.-C.G. Lanthanide Photonics: Shaping the nano world. *Trends Chem.* **2019**, *1*, 751–762. [CrossRef]
3. Bünzli, J.-C.G. *Lanthanides, Kirk-Othmer Encyclopedia of Chemical Technology*; Wiley Online Library: New York, NY, USA, 2013; pp. 1–43.
4. Cotton, S. *Lanthanide and Actinide Chemistry*; John Wiley & Sons Ltd.: Chichester, UK, 2006.
5. Harrowfield, J.M.; Silber, H.B.; Paquette, S.J. *Metal Ions in Biological Systems*; Sigel, A., Sigel, H., Eds.; Marcel Dekker: New York, NY, USA, 2003.
6. Bünzli, J.-C.G. Lanthanide luminescence for biomedical analyses and imaging. *Chem. Rev.* **2010**, *110*, 2729–2755. [CrossRef]
7. Eliseeva, S.V.; Bünzli, J.-C.G. Lanthanide luminescence for functional materials and bio-sciences. *Chem. Soc. Rev.* **2010**, *39*, 189–227. [CrossRef] [PubMed]
8. Brayshaw, L.L.; Smith, R.-C.G.; Badaoui, M.; James, A.; Irving, J.A.; Price, R.S. Lanthanides compete with calcium for binding to cadherins and inhibit cadherin-mediated cell adhesion. *Metallomics* **2019**, *11*, 914–924. [CrossRef]
9. Allen, K.N.; Imperiali, B. Lanthanide-tagged proteins—An illuminating partnership. *Curr. Opin. Chem. Biol.* **2010**, *15*, 247–254. [CrossRef]
10. Pałasz, A.; Segovia, Y.; Skowronek, R.; Worthington, J.J. Molecular neurochemistry of the lanthanides. *Synapse* **2019**, *73*, e22119. [CrossRef] [PubMed]
11. Jastrza, R.; Nowak, M.; Skrobańska, M.; Tolińska, A.; Zabiszak, M.; Gabryel, M.; Marciniak, Ł.; Kaczmarek, M.T. DNA as a target for lanthanide (III) complexes influence. *Coord. Chem. Rev.* **2019**, *382*, 145–159. [CrossRef]
12. Campello, M.P.C.; Palma, E.; Correia, I.; Paulo, P.M.R.; Matos, A.; Rino, J.; Coimbra, J.; Pessoa, J.C.; Gambino, D.; Paulo, A.; et al. Lanthanide complexes with phenanthroline-based ligands: Insights into cell death mechanisms obtained by microscopy techniques. *Dalton Trans.* **2019**, *48*, 4611–4624. [CrossRef] [PubMed]
13. Qin, Q.P.; Wang, Z.F.; Tan, M.X.; Huang, X.L.; Zou, H.H.; Zou, B.Q.; Shi, B.B.; Zhang, S.H. Complexes of lanthanides(III) with mixed 2,2′-bipyridyl and 5,7-dibromo-8-quinolinoline chelating ligands as a new class of promising anti-cancer agents. *Metallomics* **2019**, *11*, 1005–1015. [CrossRef]
14. Dos Santos, C.M.G.; Harte, A.J.; Quinn, S.J.; Gunnlaugson, T. Recent developments in the field of supramolecular lanthanide luminescent sensors and self-assemblies. *Coord. Chem. Rev.* **2008**, *252*, 2512–2527. [CrossRef]
15. Staszak, K.; Wieszczycka, K.; Marturano, V.; Tylkowski, B. Lanthanides complexes—Chiral sensing of biomolecules. *Coord. Chem. Rev.* **2019**, *397*, 76–90. [CrossRef]

16. Eliseeva, S.V.; Bünzli, J.-C.G. Rare earths: Jewels for functional materials of the future. *New J. Chem.* **2011**, *35*, 1165–1176. [CrossRef]
17. Carlos, L.D.; Ferreira, R.A.S.; De Zea Bermudez, V.; Julian-Lopez, B.; Escribano, P. Progress on lanthanide-based organic–inorganic hybrid phosphors. *Chem. Soc. Rev.* **2011**, *40*, 536–549. [CrossRef]
18. Ward, M.D. Mechanisms of sensitization of lanthanide (III)-based luminescence in transition metal/lanthanide and anthracene/lanthanide dyads. *Coord. Chem. Rev.* **2010**, *254*, 2634–2642. [CrossRef]
19. Chen, F.-F.; Chen, Z.-Q.; Bian, Z.-Q.; Huang, C.-H. Sensitized luminescence from lanthanides in d–f bimetallic complexes. *Coord. Chem. Rev.* **2010**, *254*, 991–1010. [CrossRef]
20. Cui, Y.; Yue, Y.; Qian, G.; Chen, B. Luminescent functional metal–organic frameworks. *Chem. Rev.* **2012**, *112*, 1126–1162. [CrossRef] [PubMed]
21. Huang, H.; Gao, W.; Zhang, X.-M.; Zhou, A.-M.; Liu, J.-P. 3D LnIII-MOFs: Displaying slow magnetic relaxation and highly sensitive luminescence sensing of alkylamines. *CrystEngComm* **2019**, *21*, 694–702. [CrossRef]
22. Greenspon, A.S.; Marceaux, B.L.; Hu, E.L. Robust lanthanide emitters in polyelectrolyte thin films for photonic applications. *Nanotechnology* **2018**, *29*, 075302. [CrossRef] [PubMed]
23. Forrester, P.R.; Patthey, F.; Fernandes, E.; Sblendorio, D.P.; Brune, H.; Natterer, F.D. Quantum state manipulation of single atom magnets using the hyperfine interaction. *Phys. Rev. B* **2019**, *100*, 180405. [CrossRef]
24. Coldeway, D. Storing Data in a Single Atom Proved Possible by IBM Researchers. *TechCrunch*. 9 March 2017. Available online: https://techcrunch.com/2017/03/08/storing-data-in-a-single-atom-proved-possible-by-ibm-researchers/ (accessed on 10 March 2017).
25. Hoard, R.W.; Mance, S.C.; Leber, R.L.; Dalder, E.N.; Chaplin, M.R.; Blair, K.; Nelson, D.H.; Van Dyke, D.A. Field enhancement of a 12.5-T magnet using holmium poles. *IEEE Trans. Magn.* **1985**, *21*, 448–450. [CrossRef]
26. Wollin, T.A.; Denstedt, J.D. The holmium laser in urology. *J. Clin. Laser Med. Surg.* **1998**, *16*, 13. [CrossRef] [PubMed]
27. Lucas, J.; Lucas, P.; Le Mercier, T.; Rollat, A.; Davenport, W. Rare earth doped lasers and optical amplifiers. In *Rare Earths*; Elsevier: Amsterdam, The Netherlands, 2015; pp. 319–332. [CrossRef]
28. Placer, J.; Gelabert-Mas, A.; Vallmanya, F.; Manresa, J.M.; Menéndez, V.; Cortadellas, R.; Arango, O. Holmium laser enucleation of prostate: Outcome and complications of self-taught learning curve. *Urology* **2009**, *73*, 1042–1048. [CrossRef] [PubMed]
29. Da Rosa, P.P.F.; Kitagawa, Y.; Hasegawa, Y. Luminescent lanthanide complex with seven-coordination geometry. *Coord. Chem. Rev.* **2020**, *406*, 213153. [CrossRef]
30. Hasegawa, Y.; Kitagawa, Y.; Nakanishi, T. Effective photosensitized, electrosensitized, and mechanosensitized luminescence of lanthanide complexes. *NPG Asia Mater.* **2018**, *10*, 52–70. [CrossRef]
31. Wu, D.-F.; Liu, Z.; Ren, P.; Liu, X.-H.; Wang, N.; Cui, H.-J.Z.; Gao., L. A new family of dinuclear lanthanide complexes constructed from 8-hydroxyquinoline Schiff base and β-diketone: Magnetic properties and near-infrared luminescence. *Dalton Trans.* **2019**, *48*, 1392–1403. [CrossRef] [PubMed]
32. Carlos, L.D.; Ferreira, R.A.S.; De Zea Bermudez, V.; Ribeiro, S.J.L. Lanthanide-containing light-emitting organic–inorganic hybrids: A bet on the future. *Adv. Mater.* **2009**, *21*, 509–534. [CrossRef]
33. Lis, S.; Elbanowski, M.; Makowska, B.; Hnatejko, Z. Energy transfer in solution of lanthanide complexes. *J. Photochem. Photobiol. A Chem.* **2002**, *150*, 233–247. [CrossRef]
34. De Sa, G.F.; Malto, O.L.; De Mello Donega, C.; Simas, A.M.; Longo, R.L.; Santa-Cruz, P.A.; Da Silva, E.R., Jr. Spectroscopic properties and design of highly luminescent lanthanide coordination complexes. *Coord. Chem. Rev.* **2000**, *196*, 165–195. [CrossRef]
35. Bünzli, J.-C.G.; Piguet, C. Taking advantage of luminescent lanthanide ions. *Chem. Soc. Rev.* **2005**, *34*, 1048–1077. [CrossRef]
36. Su, C.Y.; Kang, B.S.; Liu, H.Q.; Wang, Q.G.; Chen, Z.N.; Lu, Z.L.; Tong, Y.X.; Mak, T.C.W. Luminescent lanthanide complexes with encapsulating polybenzimidazole tripodal ligands. *Inorg. Chem.* **1999**, *38*, 1374–1375. [CrossRef]
37. Alpha, B.; Lehn, J.M.; Mathis, G. Energy transfer luminescence of europium(III) and terbium(III) cryptates of macrobicyclic polypyridine ligands. *Angew. Chem. Int. Ed.* **1987**, *26*, 266–267. [CrossRef]
38. Ziessel, R.; Maestri, M.; Prodi, L.; Balzani, V.; Dorsselaer, A. Dinuclear europium (3+), terbium (3+) and gadolinium (3+) complexes of a branched hexaazacyclooctadecane ligand containing six 2,2′-bipyridine pendant units. *Inorg. Chem.* **1993**, *32*, 1237–1241. [CrossRef]
39. Armelao, L.; Quici, S.; Barigelletti, F.; Accorsi, G.; Bottaio, G.; Cavazzini, M.; Tondello, E. Design of luminescent lanthanide complexes: From molecules to highly efficient photo-emitting materials. *Coord. Chem. Rev.* **2010**, *254*, 487–505. [CrossRef]
40. Binnemans, K. Rare earth β-diketonates. In *Gschneider, Design of Luminescent Lanthanide Complexes: From Molecules to Highly Efficient Photo-Emitting Materials; Handbook on the Physics and Chemistry of Rare Earths*; Bünzli, J.-C.G., Pecharsky, V.K., Eds.; Elsevier: Amsterdam, The Netherlands, 2005; Volume 35, pp. 107–272.
41. Hasegawa, Y.; Nakagawa, T.; Kawai, T. Recent progress of luminescent metal complexes with photochromic units. *Coord. Chem. Rev.* **2010**, *254*, 2643–2651. [CrossRef]
42. Yu, J.; Zhang, H.; Fu, L.; Deng, R.; Zhou, L.; Li, H.; Liu, F.; Fu, H. Synthesis, structure and luminescent properties of a new praseodymium(III) complex with β-diketone. *Inorg. Chem. Commun.* **2003**, *6*, 852–854. [CrossRef]
43. Vicente, R.; Tubau, À.; Speed, S.; Mautner, F.A.; Bierbaumer, F.; Fischer, R.C.; Massoud, S.S. Slow magnetic relaxation and luminescence properties in neodymium(III)-4,4,4-trifluoro-1-(2-naphthyl)butane-1,3-dionato complexes incorporating bipyridyl ligands. *New J. Chem.* **2021**, *45*, 14713–14723. [CrossRef]

44. Hyre, A.S.; Doerrer, L.H. A structural and spectroscopic overview of molecular lanthanide complexes with fluorinated O-donor ligands. *Coord. Chem. Rev.* **2020**, *404*, 213098. [CrossRef]
45. Gao, H.-L.; Wang, N.-N.; Wang, W.-M.; Shen, H.-Y.; Zhou, X.-P.; Chang, Y.-X.; Zhang, R.X.; Cui, J.-Z. Fine-tuning the magnetocaloric effect and SMMs behaviors of coplanar RE_4 complexes by β-diketonate coligands. *Inorg. Chem. Front.* **2017**, *4*, 860–870. [CrossRef]
46. Chang, Y.-X.; Gao, N.; Wang, M.-Y.; Wang, W.-T.; Fan, Z.-W.; Ren, D.-D.; Wu, Z.-L.; Wang, W.-M. Two phenoxo-O bridged dinuclear Dy(III) complexes exhibiting distinct slow magnetic relaxation induced by different β-diketonate ligands. *Inorg. Chim. Acta* **2020**, *505*, 119499. [CrossRef]
47. Mautner, F.A.; Bierbaumer, F.; Fischer, R.C.; Torvisco, A.; Vicente, R.; Font-Bardía, M.; Tubau, À.; Speed, S.; Massoud, S.S. Diverse coordination numbers and geometries in pyridyl adducts of lanthanide(III) complexes based on β-diketonate. *Inorganics* **2021**, *9*, 74. [CrossRef]
48. Mautner, F.A.; Bierbaumer, F.; Fischer, R.C.; Vicente, R.; Tubau, À.; Ferran, A.; Massoud, S.S. Structural characterization, magnetic and luminescent properties of praseodymium(III)-4,4,4-trifluoro-1-(2-naphthyl)butane-1,3-dionato(1-) complexes. *Crystals* **2021**, *11*, 179. [CrossRef]
49. Mautner, F.A.; Bierbaumer, F.; Gyurkac, M.; Fischer, R.C.; Torvisco, A.; Massoud, S.S.; Vicente, R. Synthesis and characterization of lanthanum(III) complexes containing 4,4,4-trifluoro-1-(2-naphthalen-yl)-butane-1,3-dionate. *Polyhedron* **2020**, *179*, 114384. [CrossRef]
50. Zhang, S.; Ke, H.; Shi, Q.; Zhang, J.; Yang, Q.; Wei, Q.; Xie, G.; Wang, W.; Yang, D.; Chen, S. Dysprosium(iii) complexes with a square-antiprism configuration featuring mononuclear single-molecule magnetic behaviours based on different β-diketonate ligands and auxiliary ligands. *Dalton Trans.* **2016**, *45*, 5310–5320. [CrossRef]
51. Li, D.-P.; Zhang, X.-P.; Wang, T.-W.; Ma, B.-B.; Li, C.-H.; Li, Y.-Z.; You, X.-Z.; You, X.-Z. Distinct magnetic dynamic behavior for two polymorphs of the same Dy(III) complex. *Chem. Commun.* **2011**, *47*, 6867–6869. [CrossRef] [PubMed]
52. Yu, J.; Deng, R.; Sun, L.; Li, Z.; Zhang, H. Photophysical properties of a series of high luminescent europium complexes with fluorinated ligands. *J. Lumin.* **2011**, *131*, 328–335. [CrossRef]
53. Fernandes, J.A.; Ferreira, R.A.S.; Pillinger, M.; Carlos, L.D.; Jepsen, J.; Hazell, A.; Ribeiro-Claro, P.; Goncalves, I.S. Investigation of europium(III) and gadolinium(III) complexes with naphthoyltrifluoroacetone and bidentate heterocyclic amines. *J. Lumin.* **2005**, *113*, 50–63. [CrossRef]
54. Thompson, L.C.; Atchison, F.W.; Young, V.G. Isomerism in the adduct of tris(4, 4,4,-trifluoro-1-(2-naphthyl)-1,3-butanedionato) europium(III) with dipyridyl. *J. Alloys Compd.* **1998**, *275*, 765–768. [CrossRef]
55. Trieu, T.-N.; Dinh, T.-H.; Nguyen, H.-H.; Abram, U.; Nguyen, M.-H. Novel lanthanoide(III) ternary complexes with naphtoyltrifluoroacetone: A synthetic and spectroscopic study. *Z. Anorg. Allg. Chem.* **2015**, *641*, 1934–1940. [CrossRef]
56. Taydakov, I.V.; Akkuzina, A.; Avetisov, R.I.; Khomyakov, A.V.; Saifutarov, R.R.; Avetissov, I.C. Effective electroluminescent materials for OLED applications based on lanthanide 1,3-diketonates bearing pyrazole moiety. *J. Lumin.* **2016**, *177*, 31–39. [CrossRef]
57. Maggini, I.; Traboulsi, H.; Yoosaf, K.; Mohanraj, J.; Wouters, J.; Pietraszkiewicz, O.; Pietraszkiewicz, M.; Armaroli, N.; Bonifazi, D. Electrostatically-driven assembly of MWCNTs with a europium complex. *Chem. Commun.* **2011**, *47*, 1625–1627. [CrossRef] [PubMed]
58. Lunstroot, L.; Nockemann, P.; Van Hecke, K.; Van Meervelt, L.; Gorller-Walrand, C.; Binnemans, K.; Driesen, K. Visible and near-infrared emission by samarium (III)-containing ionic liquid mixtures. *Inorg. Chem.* **2009**, *48*, 3018–3026. [CrossRef] [PubMed]
59. Bruno, S.M.; Ferreira, R.A.S.; Paz, F.A.A.; Carlos, L.D.; Pillinger, M.; Ribeiro-Claro, P.; Goncalves, I.S. Structural and photoluminescence studies of a europium(III) tetrakis(β-diketonate) complex with tetrabutylammonium, imidazolium, pyridinium and silica-supported imidazolium counterions. *Inorg. Chem.* **2009**, *48*, 4882–4895. [CrossRef] [PubMed]
60. Tu, H.-R.; Sun, W.-B.; Li, H.-F.; Chen, P.; Tian, Y.-M.; Zhang, W.-Y.; Zhang, Y.-Q.; Yan, P.-F. Complementation and joint contribution of appropriate intramolecular coupling and local ion symmetry to improve magnetic relaxation in a series of dinuclear Dy2 single-molecule magnets. *Inorg. Chem. Front.* **2017**, *4*, 499–508. [CrossRef]
61. Martin-Ramos, P.; Coya, C.; Alvarez, A.L.; Ramos-Silva, M.; Zaldo, C.; Paixao, J.A.; Chamorro-Posada, P.; Martin-Gil, J. Charge transport and sensitized 1.5 μm electroluminescence properties of full solution-processed NIR-OLED based on novel Er(III) fluorinated β-diketonate ternary complex. *J. Phys. Chem. C* **2013**, *117*, 10020–10030. [CrossRef]
62. Dasari, S.; Singh, S.; Sivakumar, S.; Patra, A.K. Dual-sensitized luminescent europium(III) and terbium(III) complexes as bioimaging and light-responsive therapeutic agents. *Chem. Eur. J.* **2016**, *22*, 7387–17396. [CrossRef]
63. Bruno, S.M.; Ananias, D.; Paz, F.A.A.; Pillinger, M.; Valente, A.A.; Carlos, L.D.; Goncalves, I.S. Crystal structure and temperature-dependent luminescence of a heterotetranuclear sodium–europium(III) β-diketonate complex. *Dalton Trans.* **2015**, *44*, 488–492. [CrossRef]
64. Fernandes, J.A.; Braga, S.S.; Pillinger, M.; Ferreira, R.A.S.; Carlos, L.D.; Hazell, A.; Ribeiro-Claro, P.; Goncalves, I.S. β-Cyclodextrin inclusion of europium(III) tris(β-diketonate)-bipyridine. *Polyhedron* **2006**, *25*, 1471–1476. [CrossRef]
65. Shen, F.; Hu, J.; Xie, M.; Wang, S.; Huang, X. Synthesis and structural investigation of lanthanide organometallics involving cyclopentadienyl and 2-napthoyltrifluoroacetonato chelate ligands Synthesis and structural investigation of lanthanide organometallics involving cyclopentadienyl and 2-napthoyl-trifluoroacetonato chelate ligands. *J. Organomet. Chem.* **1995**, *485*, C6–C9.

66. Shen, F.; Hu, J.; Xie, M.; Wang, S.; Huang, X. Synthesis and structural study of cyclopentadienyl lanthanide derivatives containing the 2-naphthoyltrifluoro-acetonato ligand. *Polyhedron* **1996**, *15*, 1151–1155. [CrossRef]
67. Bruker. *APEX, SAINT v. 8.37A*; Bruker AXS, Inc.: Madison, WI, USA, 2015.
68. Sheldrick, G.M. *SADABS v. 2*; University of Goettingen: Goettingen, Germany, 2001.
69. Sheldrick, G.M. A Short history of SHELX. *Acta Crystallogr. A* **2008**, *64*, 112–122. [CrossRef]
70. Sheldrick, G.M. Crystal structure refinement with SHELXL. *Acta Crystallogr. C Struct. Chem.* **2015**, *71*, 3–8. [CrossRef]
71. Macrae, C.F.; Edington, P.R.; McCabe, P.; Pidcock, E.; Shields, G.P.; Taylor, R.; Towler, T.; Van de Streek, J.J. Mercury: Visualization and analysis of crystal structures. *Appl. Cryst.* **2006**, *39*, 453–457. [CrossRef]
72. Spek, A.L. *PLATON, a Multipurpose Crystallographic Tool*; Utrecht University: Utrecht, The Netherlands, 1999.
73. Alvarez, S.; Alemany, P.; Casanova, D.; Cirera, J.; Llunell, M.; Avnir, D. Shape maps and polyhedral interconversion paths in transition metal chemistry. *Chem. Soc. Rev.* **2005**, *249*, 1693–1708. [CrossRef]
74. Cirera, J.; Alvarez, S. Stereospinomers of pentacoordinate iron porphyrin complexes: The case of the [Fe(porphyrinato)(CN)]$^{-}$ anions. *Dalton Trans.* **2013**, *42*, 7002–7008. [CrossRef]
75. Boyer, J.C.; Vetrone, F.; Capobianco, J.A.; Speghini, A.; Zambelli, M.; Bettinelli, M. Investigation of the upconversion processes in nanocrystalline $Gd_3Ga_5O_{12}$:Ho^{3+}. *J. Lumin.* **2004**, *106*, 263–268. [CrossRef]
76. Zhang, T.; Wang, J.; Jiang, J.; Pan, R.; Zhang, B. Microstructure and photoluminescence properties of Ho-doped (Ba,Sr)TiO_3 thin films. *Thin Solid Films* **2007**, *515*, 7721–7725. [CrossRef]
77. Lim, C.S.; Aleksandrovsky, A.; Molokeev, M.; Oreshonkov, A.; Atuchin, V. The modulated structure and frequency upconversion properties of $CaLa_2$ $(MoO_4)_4$: Ho^{3+}/Yb^{3+} phosphors prepared by microwave synthesis. *Phys. Chem. Chem. Phys.* **2015**, *17*, 19278–19287. [CrossRef]
78. Susumu, S.; Masanobu, W. Relations between intramolecular energy transfer efficiencies and triplet state energies in rare earth β-diketone chelates. *Bull. Chem. Soc. Jpn.* **1970**, *43*, 1955–1962.
79. Latva, M.; Takalo, H.; Mukkala, V.-M.; Matachescu, C.; Rodríguez-Ubis, J.C.; Kankare, J. Luminescent Lanthanoid Calixarene Complexes and Materials. *J. Lumin.* **1997**, *75*, 149–169. [CrossRef]
80. Quici, S.; Cavazzini, M.; Marzanni, G.; Accorsi, G.; Armaroli, N.; Ventura, B.; Barigelletti, F. Visible and near-infrared intense luminescence from water-soluble lanthanide [Tb(III), Eu(III), Sm(III), Dy(III), Pr(III), Ho(III), Yb(III), Nd(III), Er(III)] complexes. *Inorg. Chem.* **2005**, *44*, 529–537. [CrossRef] [PubMed]
81. Komissar, D.A.; Metlin, M.T.; Ambrozevich, S.A.; Taydakov, I.V.; Tobokhova, A.S.; Varaksina, E.A.; Selyukov, A.S. Luminescence properties of pyrazolic 1,3-diketone Ho^{3+} complex with 1,10-phenanthroline. *Spectrochim. Acta Part A Mol. Biomol. Spectrosc.* **2019**, *222*, 117229–117238. [CrossRef]
82. Dang, S.; Yu, J.; Yu, J.; Wang, X.; Sun, L.; Feng, J.; Fan, W.; Zhang, H. Novel holmium (Ho) and praseodymium (Pr) ternary complexes with fluorinated-ligand and 4,5-diazafluoren-9-one. *Mater. Lett.* **2011**, *65*, 1642–1644. [CrossRef]
83. Dang, S.; Sun, L.-N.; Song, S.-Y.; Zhang, H.-J.; Zheng, G.-L.; Bi, Y.-F.; Guo, H.-D.; Guo, Z.-Y.; Feng, J. Syntheses, crystal structures and near-infrared luminescent properties of holmium (Ho) and praseodymium (Pr) ternary complexes. *Inorg. Chem. Commun.* **2008**, *11*, 531–534. [CrossRef]
84. Coban, M.B.; Amjad, A.; Aygun, M.; Kara, H. Sensitization of HoIII and SmIII luminescence by efficient energy transfer from antenna ligands: Magnetic, visible and NIR photoluminescence properties of GdIII, HoIII and SmIII coordination polymers. *Inorg. Chim. Acta* **2017**, *455*, 25–33.
85. Ahmed, Z. Iftikhar, K. Sensitization of visible and NIR emitting lanthanide(III) ions in noncentrosymmetric complexes of hexafluoroacetylacetone and unsubstituted monodentate pyrazole. *Phys. Chem. A* **2013**, *117*, 11183–11201. [CrossRef] [PubMed]
86. Atwood, D.A. (Ed.) *The Rare Earth Elements: Fundamentals and Applications*; John Wiley & Sons Ltd.: Chichester, UK, 2005.